Published in final edited form as:
Cancer Res. 2021 December 01; 81(23): 6004–6017. doi:10.1158/0008-5472.CAN-21-1499.

Hyperpolarized carbon-13 MRI for early response assessment of neoadjuvant chemotherapy in breast cancer patients

Ramona Woitek[a,b,c,d], **Mary McLean**[b,e], **Stephan Ursprung**[a,b], **Oscar M Rueda**[e,f], **Raquel Manzano Garcia**[e], **Matthew Locke**[a,b], **Lucian Beer**[a,b,d], **Gabrielle Baxter**[b], **Leonardo Rundo**[a,b], **Elena Provenzano**[a,m], **Joshua Kaggie**[b], **Andrew Patterson**[c], **Amy Frary**[a,b], **Johanna Field-Rayner**[a,b], **Vasiliki Papalouka**[c], **Justine Kane**[g,m], **Arnold Benjamin**[a,b], **Andrew B Gill**[b], **Andrew Priest**[b], **David Lewis**[i,j], **Roslin Russell**[e], **Ashley Grimmer**[a,b], **Brian White**[a,b], **Beth Latimer-Bowman**[a,b], **Ilse Patterson**[c], **Amy Schiller**[c], **Bruno Carmo**[c], **Rhys Slough**[c], **Titus Lanz**[k], **James Wason**[f,h], **Rolf Schulte**[l], **Suet-Feung Chin**[e], **Martin J Graves**[b,c], **Fiona J Gilbert**[a,b,c], **Jean E Abraham**[g,m], **Carlos Caldas**[e,g,m], **Kevin M Brindle**[e,n], **Evis Sala**[a,b,c], **Ferdia A Gallagher**[a,b,c]

[a]Cancer Research UK Cambridge Centre, University of Cambridge, Cambridge, UK

[b]Department of Radiology, University of Cambridge, Cambridge, UK

[c]Department of Radiology, Addenbrooke's Hospital, Cambridge University Hospitals NHS Foundation Trust, Cambridge, UK

[d]Department of Biomedical Imaging and Image-guided Therapy, Medical University of Vienna, Vienna, Austria

[e]Cancer Research UK Cambridge Institute, University of Cambridge, Li Ka Shing Centre, Cambridge, UK

[f]MRC Biostatistics Unit, University of Cambridge, Cambridge, UK

[g]Department of Oncology, Addenbrooke's Hospital, Cambridge University Hospitals NHS Foundation Trust, Cambridge, England

[h]Population Health Sciences Institute, Newcastle University, Newcastle-upon-Tyne, UK

[i]Molecular Imaging Laboratory Cancer Research UK Beatson Institute, Glasgow, UK

[j]Institute of Cancer Sciences, University of Glasgow, Glasgow, UK

[k]RAPID Biomedical, Rimpar, Germany

Correspondence to: Ferdia A Gallagher.

Corresponding author: Ferdia Gallagher, Department of Radiology, University of Cambridge School of Clinical Medicine, Box 218 Cambridge Biomedical Campus, Cambridge, United Kingdom fag1000@cam.ac.uk, +44 1223 467062.

Author Contributions

R.W., M.M., S.U., O.M.R., R.M.G., M.L., L.B., S.-F. C., M.J.G., F.J.G., J.E.A., C.C., K.M.B., E.S. and F.A.G. contributed to study design, data acquisition, data analysis, and writing and proofreading of the manuscript. G.B., L.R., J.K., A.P., A.F., J.F.-R., V.P., J.K., A.B., A.B.G., A.P., D.L., R.R., A.G., B.W., B.L.-B., I.P., A.S., B.C., R.S., T.L., J.W., and R.S. contributed to data acquisition, data analysis and proofreading of the manuscript.

Competing Interests

F.A.G. and K.M.B. hold research agreements with GE Healthcare.

Europe PMC Funders Author Manuscripts

[l]GE Healthcare, Munich, Germany

[m]Cambridge Breast Cancer Research Unit, Department of Oncology, Addenbrooke's Hospital, Cambridge University Hospitals NHS Foundation Trust, Cambridge, UK

[n]Department of Biochemistry, University of Cambridge, Cambridge, UK

Abstract

Hyperpolarized ^{13}C-magnetic resonance imaging (MRI) is an emerging tool for probing tissue metabolism by measuring ^{13}C-label exchange between intravenously injected hyperpolarized [1-^{13}C]pyruvate and endogenous tissue lactate. Here we demonstrate that hyperpolarized ^{13}C-MRI can be used to detect early response to neoadjuvant therapy in breast cancer. Seven patients underwent multiparametric ^{1}H-MRI and hyperpolarized ^{13}C-MRI before and 7-11 days after commencing treatment. An increase in the lactate-to-pyruvate ratio of ~20% identified three patients who, following 5-6 cycles of treatment, showed pathological complete response. This ratio correlated with gene expression of the pyruvate transporter *MCT1*, and lactate dehydrogenase A (*LDHA*), the enzyme catalyzing label exchange between pyruvate and lactate. Analysis of ~2000 breast tumors showed that overexpression of *LDHA* and the hypoxia marker *CAIX* were associated with reduced relapse-free and overall survival. Hyperpolarized ^{13}C-MRI represents a promising method for monitoring very early treatment response in breast cancer and has demonstrated prognostic potential.

Keywords

Breast cancer; hyperpolarized magnetic resonance imaging; metabolic imaging; molecular imaging; neoadjuvant treatment; neoadjuvant chemotherapy

Introduction

Neoadjuvant chemotherapy (NACT) is the standard-of-care treatment for 17-40% of patients with operable early-stage breast cancer, particularly patients with HER2-positive (HER2+) and triple-negative breast cancer (TNBC) (1). NACT can be used in downstaging of locally advanced breast cancer when breast conservation is considered and in testing of novel drugs. Pathological complete response (pCR) at surgery indicates a favorable prognosis and rates of pCR have recently been shown to reach 68-80% in patients receiving carboplatin or dual HER2 blockade (2). The response to NACT can guide decisions regarding additional adjuvant systemic therapy in non-responders (3,4) or de-escalation of therapy if an early response is identified (5).

Early prediction of pCR on imaging can be used to decrease side effects from non-efficacious drugs in non-responders and could allow these patients to receive alternative regimens or investigational agents. Although early response assessment in breast cancer can be undertaken with multiparametric proton MRI (^{1}H-MRI) using dynamic contrast-enhanced MRI (DCE-MRI) and diffusion-weighted imaging (DWI), a recent meta-analysis demonstrated substantial heterogeneity in sensitivity and specificity between studies (6,7).

Aggressive breast cancers, such as HER2+ and TNBC, often switch to glycolysis, either as a result of aerobic glycolysis (the Warburg effect) or due to hypoxia, leading to increased intratumoral lactate production (8–10). This switch can be detected by intravenous injection of hyperpolarized [1-^{13}C]pyruvate and monitoring the subsequent exchange of hyperpolarized ^{13}C-label between pyruvate and lactate using ^{13}C magnetic resonance imaging (MRI). This experimental clinical imaging tool has been explored in a number of cancer types (11–16). We have demonstrated the feasibility of using hyperpolarized ^{13}C-MRI to assess patients with different subtypes of breast cancer, where higher levels of lactate labelling were observed in higher grade tumors, including TNBCs (11). In the majority of preclinical studies to date, successful treatment response was demonstrated by a decrease in tumor lactate labelling, which can be observed as early as 24 hours after cytotoxic treatment in a range of cancer models, including breast cancer (17). However, in a small number of animal studies the opposite effect occurred, with an increase in ^{13}C-lactate signal following a successful response to therapy (18,19). We have also recently described the first clinical example of response assessment in human breast cancer following NACT using hyperpolarized ^{13}C-MRI, showing a decreased flux of hyperpolarized ^{13}C-label into lactate after one complete NACT cycle of 3 weeks. Dynamic contrast-enhanced (DCE) MRI in this patient incorrectly predicted a poor response to therapy (16). Important questions remain about the temporal changes in lactate labelling and how widely applicable this response is across patients and tumor types.

Most studies define early response in breast cancer as that observed after a full cycle or several weeks of NACT (6). We have previously used a similar time point for the first proof of principle study in which hyperpolarized ^{13}C-MRI was used to monitor treatment response in breast cancer (16). However, there is an unmet need for very early response assessment in breast cancer patients, ideally within days or a week of treatment, to allow patients to rapidly change to the most appropriate treatment. Hyperpolarized ^{13}C-MRI is a promising candidate technique for this very early response assessment as metabolic changes in response to treatment have been shown to occur on this timescale (17,20–22). This prospective clinical study was designed to assess the potential added value of hyperpolarized ^{13}C-MRI for very early response assessment in patients with aggressive breast cancer (TNBC or HER2+) undergoing neoadjuvant treatment in comparison with advanced multiparametric proton MRI techniques. The aim was to determine if responders could be identified by an early change in lactate ^{13}C-labelling. We have also explored the relationship between lactate labelling in individual patients and the expression, at an RNA level, of those genes that may influence pyruvate metabolism, demonstrating the prognostic significance of this pattern of gene expression in a large group of breast cancer patients.

Materials and Methods

Patient Recruitment

Local research ethics committee approval was obtained for this prospective study (National Research Ethics Service Committee East of England, Cambridge South, Research Ethics Committee number 15/EE/0378; National Institute for Health Research [NIHR] portfolio number 30388). Written informed consent was obtained from seven patients diagnosed with

invasive carcinoma of the breast between 2018 and 2020. Data for the baseline exam of one of these patients were included in a previous publication (11).

Pathological complete response (pCR) was defined as the absence of residual invasive carcinoma in the resected breast specimen at surgery, regardless of the presence of ductal carcinoma *in situ* (DCIS).

MRI

Multinuclear breast MRI including ^{13}C-MRI with hyperpolarized [1-^{13}C]pyruvate was performed at baseline prior to treatment initiation (median number of days between baseline ^{13}C-MRI and treatment initiation was 4). For one of the baseline scans, the ^{1}H-MRI was performed four days prior to the ^{13}C-MRI for technical reasons. Early follow-up scans for response assessment including ^{13}C-MRI were performed 7–11 days after the first dose of NACT was administered (median = 7 days).

^{1}H-MRI and postprocessing

All patients underwent proton breast MRI on a clinical 3 T scanner (MR750, GE Healthcare). The inbuilt ^{1}H body coil was used to acquire three-dimensional (3D) fast gradient echo scout images and subsequently T_1-weighted axial and coronal fast spoiled gradient echo images were used to plan the subsequent ^{13}C-MRI (for specifications see Supplementary Materials). After completion of ^{13}C-MRI, diagnostic quality proton breast MRI was undertaken in the prone position using a dedicated eight-channel phased array receive-only breast coil as described previously (11,23). Details regarding acquisition, reconstruction and analysis of dynamic contrast-enhanced (DCE) MRI and diffusion weighted MRI are provided in the Supplementary Materials.

^{13}C-MRI and postprocessing

Details regarding pharmacy kit and pyruvate sample preparation and hyperpolarization are provided in the Supplementary Materials.

In five patients, spectral-spatial ^{13}C-imaging was performed (patients 2, 4, 5, 6, and 7 in Supplementary Table 1). A 22.4 ms excitation with flyback gradients was applied (24), alternating between a 15-degree pulse at the pyruvate frequency and a 40-degree pulse at the lactate frequency, each followed by a single-shot spiral readout (40x40 points, 20 cm FOV, TR 2 s, time resolution 4 s).

In one patient (patient 1, Supplementary Table 1), images were acquired using a dynamic coronal iterative decomposition with echo asymmetry and least-squares estimation (IDEAL) spiral chemical shift imaging sequence (25) and data were processed as described previously (11). Baseline data of this patient were included in a previous publication (11). In another patient (patient 3, Supplementary Table 1), only spectral data at a temporal resolution of 16 s were acquired at baseline due to a technical failure; the same scanning approach was repeated at follow up to allow direct comparison. Due to the low temporal resolution in this case, LAC/PYR was calculated based on the summed spectra and this patient was excluded from any summed SNR analyses due to lack of imaging data and from apparent

Europe PMC Funders Author Manuscripts

exchange rate constant for pyruvate-lactate exchange (k_{PL}) analyses due to low temporal resolution. Although the ^{13}C-MRI technique varied between patients, it was the same for the baseline and follow-up examination in each patient (no intra-patient variation) to compare measurements between time points for the purpose of response assessment.

Signal-to-noise ratios (SNR) for pyruvate and lactate summed over time and the summed lactate-to-pyruvate ratio (LAC/PYR) were calculated from the sum-of-squares (SOS) image reconstructions (summed SNR_{PYR}, summed SNR_{LAC}, LAC/PYR; Supplementary Table 2). k_{PL} was computed using singular value decomposition (SVD) image reconstructions (k_{PL}; Supplementary Table 2) (26). Further details regarding SOS and SVD reconstructions and analysis of ^{13}C-images are provided in the Supplementary Materials.

Statistical analysis

Statistical analyses were performed using R (version 3.6.3; R Foundation). Relationships between variables were assessed using Pearson's correlation including the correlation coefficient *r*. Differences between measurements were compared using a two-sided Student's *t*-test (paired if measurements for the same patients at baseline were compared with the follow-up). *P* values below 0.05 were considered significant. No multiple testing correction was applied: Significant tests should be interpreted as exploratory rather than confirmatory.

RNA sequencing

Biopsy samples were obtained within the Personalised Breast Cancer Programme. For biopsy samples of patients included in this study, RNA was extracted from frozen tumor tissue sections obtained using the QIAGEN AllPrep DNA/RNA Mini Kit (catalog no. 80204; QIAGEN; Supplementary Materials). RNA quantification was performed using Qubit RNA BR (Invitrogen/ThermoFisher Scientific catalog no: Q10211). Assessment of the RNA integrity number was performed using a TapeStation RNA ScreenTape (Agilent Technologies).

RNA sequencing libraries were constructed using the TruSeq Stranded Total RNA Gold library preparation kit (Illumina). The libraries were sequenced as paired-end reads (2 × 75 cycles) on a HiSeq2500 platform to give a mean coverage of 150×. Gene count data were postprocessed included normalization, scaling, and the correction of library preparation effects (Supplementary Materials). In brief, Salmon version 0.14.1 was employed to estimate gene expression. The resulting estimated counts were corrected for library size and gene length. Potential library preparation bias was corrected for and further normalization was applied transforming the values to log-2 counts for linear modelling. For correlations between RNA expression data and imaging data (LAC/PYR) in our cohort of breast cancer patients, we only included patients with identical image acquisition (patients 1 and 3 were excluded, Supplementary Table 1).

METABRIC data

The expression for relevant genes in the METABRIC cohort was normalized, as described previously (27). Log-intensities were standardized using z-scores. Follow-up data and

relapse information from METABRIC was curated and processed as described recently (28). The smoothed scatterplots and Pearson correlation coefficients in Figure 5 were computed between each pair of variables, and the cor.test function in base R was used to test the hypothesis of no correlation. Further details regarding survival analysis are provided in Supplementary Materials.

Results

Seven patients with a histopathological diagnosis of early-stage breast cancer were enrolled, i.e. tumors confined to the breast, with or without locoregional lymph node involvement, but no distant metastatic disease. These included four patients with triple negative breast cancer (ER and PR negativity defined as Allred score 0 to 3); three of which were invasive cancers of no specific type [IC NST] and one apocrine invasive cancer); and three HER2+ breast cancer patients (two of which were ER+PR+, and one ER-PR-). All patients underwent standard-of-care neoadjuvant chemotherapy, patients with HER2+ breast cancer received dual anti-HER2 therapy in addition to chemotherapy, and two patients with TNBC received additional olaparib, a Poly(ADP-ribose) polymerase 1/2 (PARP1/2) inhibitor, as part of a clinical trial (PARTNER Trial, a randomized, phase II/III trial to evaluate the safety and efficacy of the addition of olaparib to platinum-based neoadjuvant chemotherapy in breast cancer patients with TNBC and/or germline *BRCA1/2* mutations). After 5-7 cycles of neoadjuvant treatment, three patients demonstrated pCR and four patients non-pCR. Of the three patients with eventual pCR, there was one ER-PR-HER+ and two ER-PR-HER2- patients (one with additional olaparib treatment and one without). Further details regarding patient and cancer characteristics and the prescribed treatments are provided in Supplementary Table 1.

Breast MRI was performed at baseline, prior to treatment initiation (median of 4 days between baseline ^{13}C-MRI and treatment initiation), and as early follow-up for response assessment at 7–11 days after the first dose of NACT was administered (median = 7 days). Examples of one responder and one non-responder imaged at these time points are shown in Figure 1. Patient age at baseline was not significantly different between patients with eventual pCR and non-pCR ($P > 0.05$).

^{13}C-MRI analysis

Mean values of ^{13}C-MRI parameters computed for all voxels in each manually drawn region of interest (ROI) were analyzed. The number of voxels included in the ^{13}C-MRI tumor ROIs ranged from 43 to 247 (mean = 102; median = 125). Results of the ^{13}C-MRI and ^{1}H-MRI data for all patients are shown in Supplementary Table 2.

Mean summed signal-to-noise ratio of pyruvate (summed SNR_{PYR}) and lactate (summed SNR_{LAC}) decreased between baseline and response assessment (summed SNR_{PYR} at baseline, mean ± standard deviation (SD) = 19.7 ± 19.9; versus 16.5 ± 21.9 at response assessment; summed SNR_{LAC} at baseline 7.0 ± 5.6 versus 4.5 ± 3.3 at response assessment) while LAC/PYR and k_{PL} increased (LAC/PYR at baseline, mean ± SD = 0.28 ± 0.17 versus 0.34 ± 0.19 at response assessment; k_{PL} at baseline 0.0064 ± 0.0058 versus 0.0079 ± 0.0078 at response assessment); however, these changes were not significant ($P > 0.05$).

Results for these parameters and those derived from ^{1}H-MRI are shown in Figure 2 for the entire cohort, and for responders and non-responders separately in Figure 3. An increase of ≥20% in LAC/PYR measured using hyperpolarized ^{13}C-MRI 7-11 days after commencing treatment, correctly predicted the three patients with eventual pCR at surgery. All patients with a change in LAC/PYR between baseline and early response assessment that was below a threshold of a 20% increase, demonstrated non-pCR at surgery (Figure 4A). The only non-responder with a change in LAC/PYR above this threshold received PARP inhibitor treatment in addition to standard therapy. For the two patients treated with a PARP inhibitor, the responder showed a higher increase in LAC/PYR than the non-responder. A similar threshold of -15% for k_{PL} separated responders (above threshold) from non-responders (below threshold), with the patient on PARP inhibition described above being the only non-responder with an increase above this threshold (Figure 4B). For the two patients receiving PARP inhibition, the increase in k_{PL} was again larger in the responder than the non-responder. k_{PL} could not be calculated in one patient due to technical reasons. Changes in LAC/PYR and k_{PL} did not differ significantly between responders and non-responders in this small cohort (P = 0.165 and P = 0.532, respectively). Neither changes in the summed SNR_{LAC} nor summed SNR_{PYR} could be used to distinguish between responders and non-responders. Of note, changes in summed SNR_{PYR} may not only reflect biological changes such as perfusion and transport, but may also represent technical differences in polarization and coil sensitivity, and should therefore be interpreted with caution.

^{1}H-MRI: volume, dynamic contrast-enhancement and diffusion-weighted imaging

HER2+ tumors were larger than TNBC at baseline (mean ± SD = 7.4 ± 3.6 mL and 2.4 ± 0.7 mL, respectively) and follow-up (4.2 ± 1.8 mL and 1.7 ± 0.2 mL, respectively) although this difference was not significant (P = 0.140 and P = 0.147, respectively). Tumor volume, as assessed on DCE-MRI, either decreased or remained stable in all tumors. Volume decreased significantly between baseline and response assessment (P = 0.04; Figure 2A) in the whole cohort, but neither tumor volume at baseline (P > 0.05) nor volume changes could be used to distinguish responders and non-responders (Figure 4E).

No significant differences in the following DCE-MRI derived pharmacokinetic parameters were identified between tumors with pCR and non-pCR, or within either group between timepoints (P > 0.05): K^{trans} (the volume transfer constant as a measure of capillary permeability to gadolinium-based contrast agent which accumulates in the extravascular extracellular tumor compartment; Figure 2G; Figure 3K and L); k_{ep} (the rate constant reflecting transfer from the extravascular extracellular tumor compartment back into the plasma); v_e (volume of the extravascular extracellular space); and $iAUC_{90}$. Change in K^{trans} was not evaluable for one patient where fat saturation failed at baseline.

The baseline perfusion fraction, *f*, measured using intravoxel incoherent motion (IVIM) was significantly lower in patients who reached pCR, compared to those with non-pCR (P = 0.026; Figure 3O and P). The tissue diffusivity (D) increased significantly in all tumors between baseline and early response assessment (P = 0.002; Figure 2B), while changes in *f* were variable. Importantly, changes in *f* and D were not significantly different between

pCR and non-pCR tumors (P = 0.946 and P = 0.861, respectively) and could not be used to distinguish the two groups (Figure 4G and H).

In the five patients with an identical ^{13}C-MRI acquisition technique at both scanning timepoints, summed SNR_{PYR}, summed SNR_{LAC}, and LAC/PYR were significantly correlated with volume as assessed on DCE-MRI (r = 0.87, P = 0.001; r = 0.68, P = 0.030; and r = -0.63, P = 0.049, respectively; Supplementary Table 3; Supplementary Figure 1). Summed SNR_{PYR} was more strongly correlated with volume than summed SNR_{LAC} resulting in a negative correlation of volume with LAC/PYR. k_{PL} was not significantly correlated with volume (r = 0.42, P = 0.231), but was positively correlated with the perfusion fraction f (r = 0.65, P = 0.044; Supplementary Figure 1). Correlations between the hyperpolarized ^{13}C-MRI parameters (summed SNR_{PYR}, summed SNR_{LAC}, LAC/PYR and k_{PL}) and the DCE-MRI parameters (K^{trans}, k_{ep}, v_e and $iAUC_{90}$) were low and non-significant (P > 0.05; Supplementary Table 3), indicating that they may be independent. Percentage changes in k_{PL} and LAC/PYR following treatment did not correlate with changes in volume or diffusion, showing that metabolic alterations were independent of size and cellularity. Percentage changes in v_e were significantly correlated with changes in LAC/PYR but not k_{PL} (r = 0.84, P = 0.035 and r = 0.14, P = 0.819 respectively). However, other DCE-MRI parameters such as K^{trans} and k_{ep} did not correlate with changes in metabolism. Importantly, changes in DCE-MRI, diffusion, and volume could not he used to correctly identify responders.

RNA expression

The hyperpolarized ^{13}C-MRI metrics LAC/PYR and k_{PL} were compared to RNA sequencing of biopsy samples at baseline, in those cases where ^{13}C-MRI was acquired using an identical acquisition technique (n = 5). We have previously demonstrated that LAC/PYR correlates with the expression of the membrane transporter for pyruvate (monocarboxylic acid transporter 1, MCT1) in a cohort of treatment-naïve breast cancers (11). Here, we also observed a significant positive correlation between LAC/PYR at baseline and expression of the solute carrier 16A1 (*SLC16A1*), the gene encoding MCT1 (r = 0.92, P = 0.028; Figure 2H) and in addition that LAC/PYR correlates with the expression of lactate dehydrogenase A (*LDHA*), the gene encoding a subunit of the enzyme LDH which catalyzes the exchange reaction between pyruvate and lactate (r = 0.90, P = 0.039; Figure 2I). Correlations of *SLC16A1* (MCT1) and *LDHA* gene expression with k_{PL} were not significant (P = 0.984 and P = 0.924, respectively). LAC/PYR and k_{PL} were not significantly correlated with gene expression of carbonic anhydrase 9 (*CAIX*) and Hypoxia Inducible Factor 1 Subunit A (*HIF1A*) (P > 0.05).

Expression of *LDHA*, *SLC16A1* (MCT1), *HIF1A* and *CAIX* and survival in different breast cancer subtypes

To further explore the significance of these findings, the intercorrelations of *LDHA*, *SLC16A1* (MCT1), *HIF1A* and *CAIX* expression were analyzed in a larger cohort, to evaluate their association with survival. Molecular Taxonomy of Breast Cancer International Consortium (METABRIC) is a large genomic and transcriptomic dataset acquired from approximately 2000 breast cancer biopsy samples (27) with its outcome update published in

2019 (28). While the expression of both, *LDHA* and *SLC16A1* (MCT1), was significantly correlated with expression of *HIF1A* and *CAIX*, the expression of *LDHA* was not significantly correlated with MCT1 (Figure 5). Overexpression of *LDHA* and the hypoxia marker *CAIX* (but not MCT1 or *HIF1A*) were also associated with poorer overall and relapse free survival (Figure 6A-H).

In addition, we also selected 501 patients from METABRIC whose breast cancer receptor status matched the patients in our imaged cohort (ER-PR-HER2- = 320 patients; ER-PR-HER2+ = 134 patients; ER+PR+HER2+ = 47 patients). While the expression of *LDHA* was significantly correlated with expression of *HIF1A* and *CAIX*, the expression of *SLC16A1* (MCT1) was not significantly correlated with either of the two in this subset of patients (Supplementary Figure 2 I). Overexpression of the hypoxia markers *CAIX* and *HIF1A* was associated with poorer overall survival and overexpression of CAIX was also associated with relapse free survival (Supplementary Figure 2 A-H).

Discussion

Most anticancer therapies induce metabolic alterations which precede the changes in tumor size that are measured routinely on standard-of-care imaging (29,30). Therefore, non-invasive methods for imaging tumor metabolism offer the possibility for earlier detection of treatment response. Hyperpolarized ^{13}C-MRI measurements using [1-^{13}C]pyruvate as a metabolic probe have shown great promise for early therapy response monitoring in a large number of preclinical cancer models, including breast cancer. We and other groups have demonstrated how lactate labelling varies with tumor grade (11,13). We have also shown that in breast cancer LAC/PYR correlates with both the expression of MCT1, which is responsible for the cellular uptake of pyruvate, and hypoxia as measured from HIF1α expression (11). To date, there have been two clinical case reports demonstrating a decrease in tumor lactate labelling following treatment in a triple negative breast cancer and a high-grade prostate cancer after 3 weeks and 6 weeks of standard-of-care therapy, respectively (16,31). The aim of this study was to evaluate the potential of hyperpolarized ^{13}C-MRI to measure very early response to therapy in breast cancer, 7-11 days after initiation of treatment, and to compare it with ^{1}H-MRI measures of vascular permeability using DCE-MRI and tissue cellularity using IVIM DWI.

The results show that an increase of ≥20% in LAC/PYR measured using hyperpolarized ^{13}C-MRI 7–11 days after commencing standard-of-care treatment correctly predicted patients with eventual pCR at surgery. Changes in no other parameter, either hyperpolarized ^{13}C-MRI or advanced multiparametric ^{1}H-MRI, could correctly identify patients with pCR. The threshold of 20% for determining response is in line with criteria, such as the Response Evaluation Criteria in Solid Tumors (RECIST) or Positron Emission Tomography Response Criteria in Solid Tumors (PERCIST), where changes higher than 20% or 30% in size or metabolism, form the basis of determining tumor progression, response, or stable disease (30,32). These results indicate that the technique holds promise for ultra-early response monitoring of NACT after 7-11 days of standard-of-care treatment, although this requires validation in larger cohorts.

The increase in LAC/PYR following treatment is interesting as the majority of preclinical hyperpolarized ^{13}C-MRI studies have reported decreased lactate labelling following a positive response to therapy (16,17,20–22,31,33). However, a treatment-induced increase in lactate labelling has been shown in a smaller number of *in vitro* and *in vivo* models (18,19,34,35). The accurate prediction of pCR with an increase in lactate labelling, rather than a decrease, raises important questions about the dynamic alterations in metabolism following treatment and the ideal timing for measuring a clinically meaningful metabolic response in future studies. Later timepoints may be dominated by opposing effects such as loss of cellularity, and this has important implications for the timing of treatment response monitoring, which are likely to be tumor- and treatment-specific.

There are a number of potential biological factors contributing to the changes in hyperpolarized ^{13}C-label exchange between pyruvate and lactate following treatment (15). For example, the intracellular pyruvate concentration is determined by both tissue perfusion and vascular delivery. Importantly, there were no significant differences in the DCE measures of vascularity (K^{trans}, v_e, or $iAUC_{90}$) between baseline and the early treatment timepoint, suggesting that pyruvate delivery via the bloodstream alone cannot account for the changes in lactate labelling. Pyruvate transport is mediated by monocarboxylate transporters (MCTs), of which MCT1 and MCT4 are the most widely expressed in human tissue. MCT1 has a greater affinity for pyruvate and is the main transmembrane transporter for hyperpolarized [1-^{13}C]pyruvate, which has been shown to be rate limiting for hyperpolarized [1-^{13}C]lactate formation in some breast cancer cell lines and can account for treatment-induced changes (19,36). We have previously demonstrated the importance of *SLC16A1* (MCT1) expression for determining lactate labelling in treatment-naïve breast tumors (11), which we have confirmed within this cohort. MCT1 has also been shown to have a role in lactate labelling in prostate cancer (13). Therefore, alterations in *SLC16A1* (MCT1) expression or its cellular localisation could account for the changes in lactate labelling seen here following treatment. The absence of a significant change in vascular permeability or K^{trans} (Figure 2G) following treatment suggests that vascular delivery of pyruvate is not responsible for the changes in LAC/PYR seen following treatment and further supports a potential role for MCT1 in these changes.

Intracellularly, the enzyme lactate dehydrogenase (LDH) catalyzes the conversion of pyruvate to lactate in the presence of the cofactor NADH. A reduction in LDH expression has been shown to mediate reduced lactate labelling in hyperpolarized ^{13}C-MRI experiments (17,22,33), as has a decrease in NADH (20,21,37), and a decrease in the intracellular lactate pool (20,34). Conversely, increasing lactate pool size and LDH expression have been shown to be associated with increasing lactate labelling after treatment (19). Here we have shown that *LDHA* expression on an individual patient level, in addition to MCT1, correlates with the LAC/PYR ratio. Taken together with the previous data we have reported, this suggests that changes in *LDHA*, in addition to MCT1, may explain the post treatment changes we have shown here.

Hypoxia may be the driver for the relationship between LAC/PYR and both MCT1 and *LDHA*, as well as the changes in LAC/PYR seen after treatment. Tissue lactate is closely related to hypoxia and we have shown previously a correlation between *HIF1A*

expression and LAC/PYR in a varied group of treatment-naïve breast cancers (11). Angiogenesis inhibitors have been shown to increase lactate labelling in a preclinical model of ovarian cancer assessed with hyperpolarized ^{13}C-MRI (18). Anti-angiogenesis is also a well-documented effect of taxanes (38) and all patients in our cohort received either weekly doses of paclitaxel or three-weekly docetaxel (Supplementary Table 1). In the absence of significant changes in the measured pharmacokinetic parameters (K^{trans}, v_e, or iAUC$_{90}$) on DCE-MRI, any changes in hypoxia are likely to be driven by cellular changes in oxygen demand rather than by changes in the vasculature. Immune cell infiltration has been shown to contribute to the uptake of the radiolabelled glucose analog [^{18}F]fluorodeoxyglucose (^{18}F-FDG) on positron emission tomography (PET) in breast cancer patients following response to hormonal therapy (39,40). An increase in tumor infiltrating immune cells in responders could therefore also increase LAC/PYR more strongly as seen in our study. Future analysis of tumor tissue at this very early response assessment timepoint will further elucidate the mechanisms responsible for the increasing LAC/PYR in responding patients. Very early treatment induced changes in cellular redox status could also contribute to these findings. For example, the early effects of treatment may generate a reducing environment with increasing NADH favoring lactate formation, whereas a later oxidized state would increase the relative concentration of NAD^+ favoring conversion from lactate to pyruvate at later stages of treatment (41). However, tissue redox status is difficult to assess in practice, particularly at multiple timepoints during treatment but future validation of our results with assays quantifying NAD+ (and protein expression of MCT1, LDHA, CAIX and HIF1A) will be important to fully understand the molecular changes underlying our imaging results.

In order to validate some of our findings in an external cohort, and to understand the clinical significance of the results, we subsequently analyzed the expression data from almost 2,000 patients in the METABRIC dataset (27,28). In addition to MCT1 and *LDHA*, *CAIX* was assessed as a stable membrane-bound isoform of the enzyme carbonic anhydrase which is upregulated in hypoxic conditions and has been shown to be important for pH regulation of tumors (42). *LDHA* and MCT1 expression was significantly correlated with expression of both hypoxia markers, *CAIX* and *HIF1A*, showing the important interrelationship between pyruvate metabolism, lactate formation and hypoxia. There was a strong correlation between overexpression of both *LDHA* and *CAIX* and a statistically significant reduction in relapse free survival and overall survival. Therefore, LAC/PYR may provide important prognostic information in addition to detection of early treatment response. It also suggests the importance of combining imaging measures of hypoxia and metabolism with histopathological metrics to more fully phenotype tumors, as well as for prognosis.

Olaparib inhibits PARP1 and 2, two enzymes functioning as DNA damage sensors and facilitators of DNA damage repair mechanisms by using NAD^+ as a substrate to polyADP-ribosylate (PARylate) themselves and other target proteins (43,44). While up to 90% of cellular NAD^+ can be used by PARPs in response to cellular DNA damage, PARP inhibitors compete with NAD^+ for the catalytic cages of PARPs and trap PARPs at DNA double strand breaks to impair PARylation and the DNA damage repair it mediates (44–46). Both patients receiving a PARP inhibitor in addition to standard-of-care treatment (one with eventual pCR and another one with non-pCR) also demonstrated an increase in LAC/PYR greater than

20%, and the increase in LAC/PYR was much higher in the patient with pCR than non-pCR, again pointing towards a greater increase in responders. PARP inhibitors have been shown to increase NAD^+ levels in both murine cells and liver tissue (47), and decreasing NAD^+ levels have been correlated with decreasing lactate labelling in hyperpolarized ^{13}C-MRI experiments previously (20,21,37). These results suggest that increasing availability of intracellular NAD(H) due to PARP inhibitor treatment may elevate LDH-mediated lactate labelling. PARP inhibitors might therefore cause a pharmacodynamic increase in LAC/PYR and k_{PL} regardless of response, and the larger increase in the patient who responded may be accounted for by additional changes in MCT1 and/or LDHA, or an increase in immune cell infiltration. A previous study in the MCF-7 breast cancer cell line has shown that lactate increases with a MEK inhibitor, which was explained by activation of the PI3K and/or AMPK pathways (34). These results suggest that caution is warranted in interpreting results in patients undergoing experimental targeted treatment where the mode of action could influence lactate production.

Pharmacokinetic parameters from DCE-MRI and diffusivity from DWI (including IVIM) have also been explored for early response prediction in breast cancer, with K^{trans} typically decreasing and diffusivity increasing in responders compared to non-responders (48–50). However, in most studies these assessments are made later during NACT than in this study. Our data showed that the perfusion fraction, f, determined using IVIM differs between pCR and non-pCR even at baseline in this cohort. A previous study found significant differences in baseline measurements of f in patients with eventual pCR when compared to those with non-pCR, although f was higher in patients with pCR in their cohort, which contrasts with our results (48). The different composition of the cohorts may account for this difference given the inclusion of mainly ER+ breast cancers previously. As with the findings from hyperpolarized ^{13}C-MRI, these IVIM-derived metrics need validation in larger cohorts. Also, diffusivity D was not found to predict pathological response in our cohort, indicating that there was no significant change in cellularity that could account for the alterations in lactate labelling at this early treatment response timepoint.

We also showed that LAC/PYR is the most reliable metric to distinguish between responders and non-responders undergoing standard-of-care treatment in our study. Results for k_{PL} were similar, although there was a smaller difference between responders and non-responders and fewer available data. As the estimation of k_{PL} depends on the SNR in images acquired at single time points, it is less accurate at lower SNR than LAC/PYR, which is calculated from the time-summed images. Our results suggest that LAC/PYR may be the most precise metric for use in the clinical setting to assess a 20% change following treatment.

The limitations of our study include the small size of the data set. The preliminary findings arising from this work will need to be confirmed and validated in larger cohorts, ideally as part of large multisite studies. However, this was a prospective study and we included patients with the two most common breast cancer subtypes who frequently undergo NACT: TNBC and HER2+. Despite the small group size, we show in both groups undergoing standard-of-care treatment that an increase of LAC/PYR of at least 20% indicates pCR and that in both the pCR and non-pCR groups there was one patient treated with a PARP

inhibitor in addition. We have explored the significance of this small dataset by analyzing the very large expression dataset within METABRIC which has shown the potential importance of the technique in demonstrating prognosis.

In conclusion, an increase in the LAC/PYR ratio of ≥20%, measured using hyperpolarized ^{13}C-MRI, has the potential to distinguish between responding and non-responding breast cancer patients undergoing standard-of-care neoadjuvant treatment as early as 7-11 days after the start of treatment. LAC/PYR is significantly correlated with both *LDHA* and *SLC16A1* (MCT1) expression in this cohort. Comparison with a large breast cancer gene expression dataset (METABRIC) showed that *LDHA* and *SLC16A1* (MCT1) expression is significantly correlated with expression of the hypoxia markers *CAIX* and *HIF1A* and that overexpression of the hypoxia marker *CAIX* and *LDHA* are significantly associated with shorter overall and relapse free survival in breast cancer.

Supplementary Material

Refer to Web version on PubMed Central for supplementary material.

Acknowledgements

This work was supported by the Mark Foundation for Cancer Research and Cancer Research UK Cambridge Centre (Grant C9685/A25177), Cancer Research UK (CRUK; Grants C8742/A18097, C19212/A16628, C19212/A27150, and C197/A16465), the Austrian Science Fund (Grant J4025-B26), the CRUK Cambridge Centre, the CRUK & Engineering and Physical Sciences Research Council Cancer Imaging Centre in Cambridge and Manchester, Addenbrooke's Charitable Trust, and the NIHR Cambridge Biomedical Research Centre (BRC-1215-20014). The NIHR Cambridge Biomedical Research Centre (BRC) is a partnership between Cambridge University Hospitals NHS Foundation Trust and the University of Cambridge, funded by the National Institute for Health Research (NIHR). The views expressed are those of the authors and not necessarily those of the NIHR or the Department of Health and Social Care. We also acknowledge funding from the UKRI Medical Research Council (MC UU 00002/16), the Cambridge Experimental Cancer Medicine Centre, a Wellcome Trust Strategic Award, and Cambridge University Hospitals National Health Service Foundation Trust. We acknowledge the support of the Cambridge Breast Cancer Research Unit Laboratory in the collection of clinical data and samples and the Cancer Molecular Diagnostics for the extraction of DNA/RNA. The PARTNER Trial (https://clinicaltrials.gov/ct2/show/NCT03150576) was supported by Cancer Research UK and AstraZeneca (CRUK/14/048 and ESR-14-10241). The Personalised Breast Cancer Program is a collaboration between CRUK Cambridge Centre and Illumina (C507/A27657). We also acknowledge and are grateful for the involvement of our patients in these research projects.

Data and Code Availability

Transcriptomic data for those tumors included in our study on hyperpolarized 13C-MRI will be deposited at the European Genome-phenome Archive (https://ega-archive.org/datasets/EGAD00001008141). Imaging raw data, and MATLAB scripts for data in this manuscript can be obtained from radiology-13c-mri-breast@lists.cam.ac.uk.

References

1. Murphy BL, Day CN, Hoskin TL, Habermann EB, Boughey JC. Neoadjuvant Chemotherapy Use in Breast Cancer is Greatest in Excellent Responders: Triple-Negative and HER2+ Subtypes. Ann Surg Oncol. 25 :2241–2248.
2. van Ramshorst MS, van der Voort A, van Werkhoven ED, Mandjes IA, Kemper I, Dezentjé VO, et al. Neoadjuvant chemotherapy with or without anthracyclines in the presence of dual HER2 blockade for HER2-positive breast cancer (TRAIN-2): a multicentre, open-label, randomised, phase 3 trial. Lancet Oncol. 19 :1630–40.

3. Masuda N, Lee S-J, Ohtani S, Im Y-H, Lee E-S, Yokota I, et al. Adjuvant Capecitabine for Breast Cancer after Preoperative Chemotherapy. N Engl J Med. 376 :2147–2159.
4. von Minckwitz G, Huang C-S, Mano MS, Loibl S, Mamounas EP, Untch M, et al. Trastuzumab Emtansine for Residual Invasive HER2-Positive Breast Cancer. N Engl J Med. 380 :617–628.
5. Cortes J, Gebhart G, Ruiz Borrego M, Stradella A, Bermejo B, Escrivá S, et al. Chemotherapy (CT) deescalation using an FDG-PET/CT (F-PET) and pathological response-adapted strategy in HER2[+] early breast cancer (EBC): PHERGain Trial. J Clin Oncol. 38 :503–503.
6. Cheng Q, Huang J, Liang J, Ma M, Ye K, Shi C, et al. The Diagnostic Performance of DCE-MRI in Evaluating the Pathological Response to Neoadjuvant Chemotherapy in Breast Cancer: A Meta-Analysis. Front Oncol. 10
7. Partridge SC, Zhang Z, Newitt DC, Gibbs JE, Chenevert TL, Rosen MA, et al. Diffusion-weighted MRI Findings Predict Pathologic Response in Neoadjuvant Treatment of Breast Cancer: The ACRIN 6698 Multicenter Trial. Radiology. 289 :618–27.
8. Castagnoli L, Iorio E, Dugo M, Koschorke A, Faraci S, Canese R, et al. Intratumor lactate levels reflect HER2 addiction status in HER2-positive breast cancer. J Cell Physiol. 234 :1768–1779.
9. Gandhi N, Das G. Metabolic Reprogramming in Breast Cancer and Its Therapeutic Implications. Cells. 8 :89.
10. Kim S, Kim DH, Jung W-H, Koo JS. Metabolic phenotypes in triple-negative breast cancer. Tumor Biol. 34 :1699–712.
11. Gallagher FA, Woitek R, McLean MA, Gill AB, Manzano Garcia R, Provenzano E, et al. Imaging breast cancer using hyperpolarized carbon-13 MRI. Proc Natl Acad Sci. 117 :2092–2098.
12. Grist JT, Miller JJ, Zaccagna F, McLean MA, Riemer F, Matys T, et al. Hyperpolarized 13C MRI: A novel approach for probing cerebral metabolism in health and neurological disease. J Cereb Blood Flow Metab. 40 :1137–1147.
13. Granlund KL, Tee SS, Vargas HA, Lyashchenko SK, Reznik E, Fine S, et al. Hyperpolarized MRI of Human Prostate Cancer Reveals Increased Lactate with Tumor Grade Driven by Monocarboxylate Transporter 1. Cell Metab. 31 :105–114. e3
14. Stødkilde-Jørgensen H, Laustsen C, Hansen ESS, Schulte R, Ardenkjaer-Larsen JH, Comment A, et al. Pilot Study Experiences With Hyperpolarized [1- 13 C]pyruvate MRI in Pancreatic Cancer Patients. J Magn Reson Imaging. 51 :961–963.
15. Woitek R, Gallagher FA. The use of hyperpolarised 13C-MRI in clinical body imaging to probe cancer metabolism. Br J Cancer. 124 :1187–1198.
16. Woitek R, McLean M, Gill AB, Grist JT, Provenzano E, Patterson AJ, et al. Hyperpolarized 13C-MRI of Tumor Metabolism Demonstrates Early Metabolic Response to Neoadjuvant Chemotherapy in Breast Cancer. Radiol Imaging Cancer. 2 (4) e200017
17. Hesketh RL, Wang J, Wright AJ, Lewis DY, Denton AE, Grenfell R, et al. Magnetic Resonance Imaging Is More Sensitive Than PET for Detecting Treatment-Induced Cell Death-Dependent Changes in Glycolysis. Cancer Res. 79 :3557–69. [PubMed: 31088837]
18. Ravoori MK, Singh SP, Lee J, Bankson JA, Kundra V. In Vivo Assessment of Ovarian Tumor Response to Tyrosine Kinase Inhibitor Pazopanib by Using Hyperpolarized 13C-Pyruvate MR Spectroscopy and 18F-FDG PET/CT Imaging in a Mouse Model. Radiology. 285 :830–8.
19. Lodi A, Woods SM, Ronen SM. Treatment with the MEK inhibitor U0126 induces decreased hyperpolarized pyruvate to lactate conversion in breast, but not prostate, cancer cells. NMR Biomed. 26 :299–306.
20. Day SE, Kettunen MI, Gallagher FA, Hu D-E, Lerche M, Wolber J, et al. Detecting tumor response to treatment using hyperpolarized ^{13}C magnetic resonance imaging and spectroscopy. Nat Med. 13 :1382–7.
21. Witney TH, Kettunen MI, Hu D, Gallagher FA, Bohndiek SE, Napolitano R, et al. Detecting treatment response in a model of human breast adenocarcinoma using hyperpolarised [1-^{13}C]pyruvate and [1,4-^{13}C2]fumarate. Br J Cancer. 103 :1400–6.
22. Ros S, Wright AJ, D'Santos P, Hu D en, Hesketh RL, Lubling Y, et al. Metabolic Imaging Detects Resistance to PI3Kα Inhibition Mediated by Persistent FOXM1 Expression in ER+ Breast Cancer. Cancer Cell. 38 :516–533. e9

23. Bedair R, Graves MJ, Patterson AJ, McLean MA, Manavaki R, Wallace T, et al. Effect of Radiofrequency Transmit Field Correction on Quantitative Dynamic Contrast-enhanced MR Imaging of the Breast at 3.0 T. Radiology. 279 :368–377.
24. Schulte RF, Sperl JI, Weidl E, Menzel MI, Janich MA, Khegai O, et al. Saturation-recovery metabolic-exchange rate imaging with hyperpolarized [1-13C] pyruvate using spectral-spatial excitation. Magn Reson Med. 69 :1209–16.
25. Wiesinger F, Weidl E, Menzel MI, Janich MA, Khegai O, Glaser SJ, et al. IDEAL spiral CSI for dynamic metabolic MR imaging of hyperpolarized [1-^{13}C]pyruvate. Magn Reson Med. 68 :8–16. [PubMed: 22127962]
26. Rodgers CT, Robson MD. Receive array magnetic resonance spectroscopy: Whitened singular value decomposition (WSVD) gives optimal bayesian solution. Magn Reson Med. 63 :881–91. [PubMed: 20373389]
27. Curtis C, Shah SP, Chin S-F, Turashvili G, Rueda OM, Dunning MJ, et al. The genomic and transcriptomic architecture of 2,000 breast tumours reveals novel subgroups. Nature. 486 :346–52. [PubMed: 22522925]
28. Rueda OM, Sammut SJ, Seoane JA, Chin SF, Caswell-Jin JL, Callari M, et al. Dynamics of breast-cancer relapse reveal late-recurring ER-positive genomic subgroups. Nature. 567 :399–404. [PubMed: 30867590]
29. Kurhanewicz J, Vigneron DB, Ardenkjaer-Larsen JH, Bankson JA, Brindle K, Cunningham CH, et al. Hyperpolarized 13C MRI: Path to Clinical Translation in Oncology. Neoplasia (United States). 21 :1–16.
30. Eisenhauer EAA, Therasse P, Bogaerts J, Schwartz LHH, Sargent D, Ford R, et al. New response evaluation criteria in solid tumours: revised RECIST guideline (version 1.1). Eur J Cancer. 45 :228–47.
31. Aggarwal R, Vigneron DB, Kurhanewicz J. Hyperpolarized 1-[^{13}C]-Pyruvate Magnetic Resonance Imaging Detects an Early Metabolic Response to Androgen Ablation Therapy in Prostate Cancer. Eur Urol. 72 :1028–9.
32. Wahl RL, Jacene H, Kasamon Y, Lodge MA. From RECIST to PERCIST: Evolving considerations for PET response criteria in solid tumors. J Nucl Med. 50 :122–50.
33. Dafni H, Larson PEZ, Hu S, Yoshihara HAI, Ward CS, Venkatesh HS, et al. Hyperpolarized 13C spectroscopic imaging informs on hypoxia-inducible factor-1 and Myc activity downstream of platelet-derived growth factor receptor. Cancer Res. 70 :7400–7410. [PubMed: 20858719]
34. Lodi A, Woods SM, Ronen SM. MR-detectable metabolic consequences of mitogen-activated protein kinase kinase (MEK) inhibition. NMR Biomed. 27 :700–8.
35. Bohndiek SE, Kettunen MI, Hu D, Brindle KM. Hyperpolarized (13)C spectroscopy detects early changes in tumor vasculature and metabolism after VEGF neutralization. Cancer Res. 72 :854–64.
36. Talia H, Galit E, Lucio F, Hadassa D. Kinetics of Hyperpolarized 13C1-pyruvate Transport and Metabolism in Living Human Breast Cancer Cells. Proc Natl Acad Sci U S A. 106 :18131–6.
37. Witney TH, Kettunen MI, Day SE, Hu D, Neves AA, Gallagher FA, et al. A comparison between radiolabeled fluorodeoxyglucose uptake and hyperpolarized (13)C-labeled pyruvate utilization as methods for detecting tumor response to treatment. Neoplasia. 11 :574–82.
38. Bocci G, Di Paolo A, Danesi R. The pharmacological bases of the antiangiogenic activity of paclitaxel. Angiogenesis. 16 :481–492.
39. Mamede M, Saga T, Ishimori T, Nakamoto Y, Sato N, Higashi T, et al. Differential uptake of 18F-fluorodeoxyglucose by experimental tumors xenografted into immunocompetent and immunodeficient mice and the effect of immunomodification. Neoplasia. 5 :179–83.
40. Mortimer JE, Dehdashti F, Siegel BA, Trinkaus K, Katzenellenbogen JA, Welch MJ. Metabolic flare: Indicator of hormone responsiveness in advanced breast cancer. J Clin Oncol. 19 :2797–803.
41. Broekgaarden M, Bulin A-L, Frederick J, Mai Z, Hasan T. Clinical Medicine Tracking Photodynamic-and Chemotherapy-Induced Redox-State Perturbations in 3D Culture Models of Pancreatic Cancer: A Tool for Identifying Therapy-Induced Metabolic Changes. J Clin Med. 8 :1399.

42. Serrao EM, Kettunen MI, Rodrigues TB, Dzien P, Wright AJ, Gopinathan A, et al. MRI with hyperpolarised [1-^{13}C]pyruvate detects advanced pancreatic preneoplasia prior to invasive disease in a mouse model. Gut. 65 :465–75. [PubMed: 26347531]
43. Livraghi L, Garber JE. PARP inhibitors in the management of breast cancer: Current data and future prospects. BMC Med. 13 :188.
44. Bian C, Zhang C, Luo T, Vyas A, Chen SH, Liu C, et al. NADP + is an endogenous PARP inhibitor in DNA damage response and tumor suppression. Nat Commun. 10 :1–14.
45. Rouleau M, Patel A, Hendzel MJ, Kaufmann SH, Poirier GG. PARP inhibition: PARP1 and beyond. Nat Rev Cancer. :293–301.
46. Liu C, Vyas A, Kassab MA, Singh AK, Yu X. The role of poly ADP-ribosylation in the first wave of DNA damage response. Nucleic Acids Res. 45 :8129–41.
47. Almeida GS, Bawn CM, Galler M, Wilson I, Thomas HD, Kyle S, et al. PARP inhibitor rucaparib induces changes in NAD levels in cells and liver tissues as assessed by MRS. NMR Biomed. 30 :2797–803.
48. Che S, Zhao X, Ou Y, Li J, Wang M, Wu B, et al. Role of the intravoxel incoherent motion diffusion weighted imaging in the pre-treatment prediction and early response monitoring to neoadjuvant chemotherapy in locally advanced breast Cancer. Medicine (Baltimore). 95
49. Bedair R, Priest AN, Patterson AJ, McLean MA, Graves MJ, Manavaki R, et al. Assessment of early treatment response to neoadjuvant chemotherapy in breast cancer using non-mono-exponential diffusion models: a feasibility study comparing the baseline and mid-treatment MRI examinations. Eur Radiol. 27 :2726–2736.
50. Tudorica A, Oh KY, Chui SY-C, Roy N, Troxell ML, Naik A, et al. Early Prediction and Evaluation of Breast Cancer Response to Neoadjuvant Chemotherapy Using Quantitative DCE-MRI. Transl Oncol. 9 :8–17. [PubMed: 26947876]

Europe PMC Funders Author Manuscripts

Europe PMC Funders Author Manuscripts

Significance

Hyperpolarized carbon-13 MRI allows response assessment in breast cancer patients after 7-11 days of neoadjuvant chemotherapy and outperformed state-of-the-art and research quantitative proton MRI techniques.

Europe PMC Funders Author Manuscripts

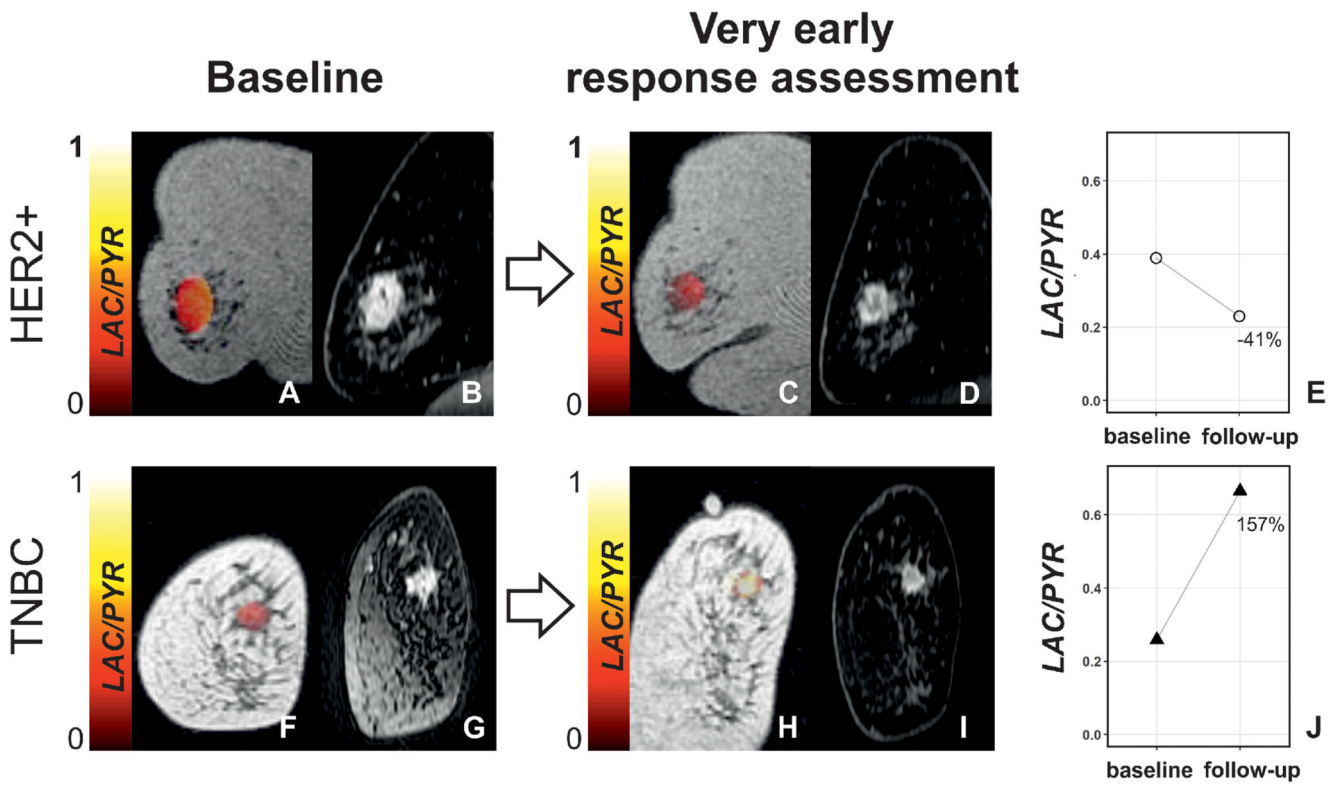

Figure 1. Changes in LAC/PYR between baseline and very early response assessment in a responder and non-responder.

(A,C,F, and H) Coronal T_1-weighted 3D spoiled gradient echo (SPGR) images with LAC/PYR map overlaid on the breast tumor. (B,D,G, and I). Coronal reformatted DCE images obtained 150 s after i.v. injection of a gadolinium-based contrast agent. A patient with HER2+ breast cancer was imaged at baseline (A and B) and for ultra-early response assessment (C and D) following standard-of-care treatment and showed a decrease in LAC/PYR of 41% (E) indicating non-response. At surgery, non-pathological complete response (non-pCR) with residual invasive cancer was identified. Another patient with TNBC was imaged at baseline (F and G) and for ultra-early response assessment (H and I) following treatment with chemotherapy and a PARP inhibitor and showed an increase in LAC/PYR of 157% (J) indicating response. At surgery, pathological complete response (pCR) without residual invasive breast cancer was found. TNBC: triple-negative breast cancer; HER2+: HER2/neu (human epidermal growth factor receptor 2) positive.

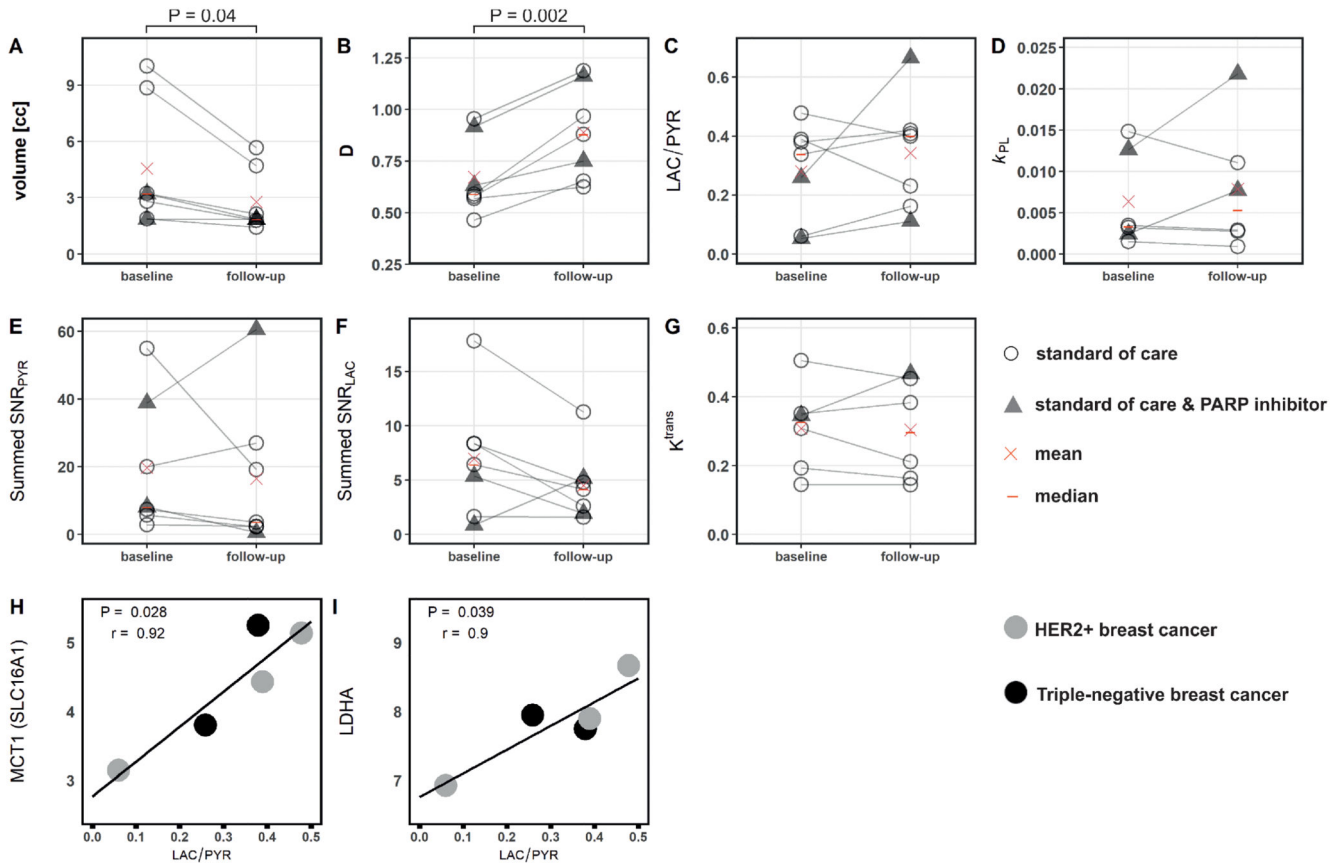

Figure 2. Parameters obtained from hyperpolarized ^{13}C-MRI and ^{1}H-MRI at baseline and in early follow up scans.

Differences between baseline and follow-up were significant for tumor volume (A) and diffusivity (B) but not for the other parameters (C-G); neither change in volume or diffusivity could distinguish pCR from non-pCR. Correlation of *SLC16A1* (MCT1) and *LDHA* mRNA expression with LAC/PYR was significant (H and I). Only images acquired with identical ^{13}C-MRI acquisition parameters (spectral-spatial excitation) were included in these correlations.

Europe PMC Funders Author Manuscripts

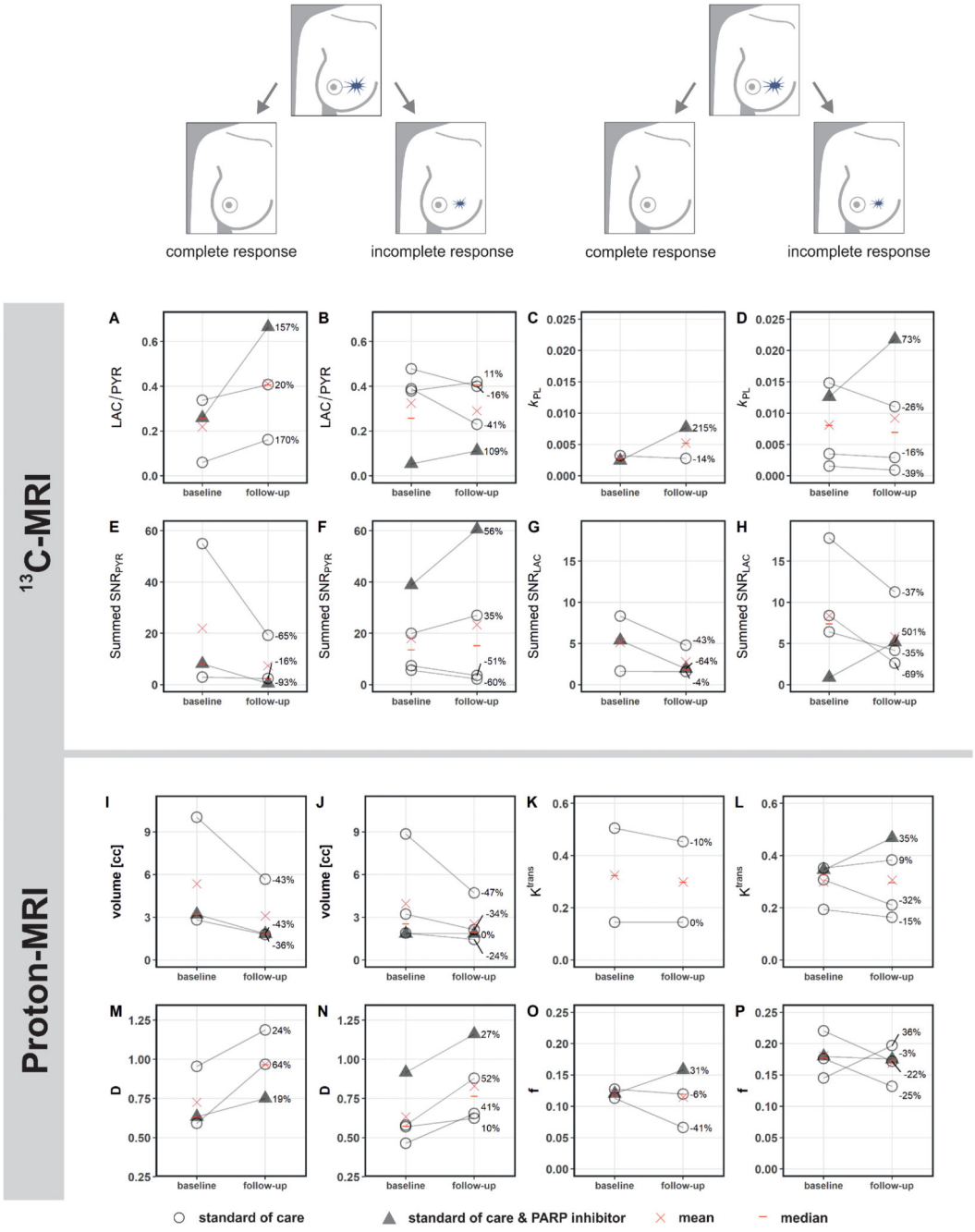

Figure 3. Changes in hyperpolarized ^{13}C- but not ^{1}H-MRI derived metrics after approximately one week of treatment distinguish responders (pathological complete response; pCR) from non-responders (incomplete response; non-pCR).

In the five patients undergoing standard-of-care neoadjuvant treatment, an increase of ≥20% in LAC/PYR was only observed in patients who responded (A), whereas a lower increase or even a decrease in LAC/PYR was observed in non-responders (B). Both patients treated with a PARP inhibitor in addition showed an increase in LAC/PYR (A and B) and again the increase was highest in the responder (A). While k_{PL} increased in all patients receiving a PARP inhibitor, but not in the other patients (C and D), neither k_{PL} nor any of the

^{1}H-MRI based metrics, from dynamic contrast-enhanced (DCE) MRI (such as K^{trans}) or from intravoxel incoherent motion (IVIM) as part of diffusion-weighted MRI (DWI; such as perfusion fraction f and tissue diffusivity D) could distinguish between responders and non-responders (I-P). None of the parameters differed significantly between baseline and follow-up when evaluated for responders and non-responders separately ($P > 0.05$). k_{PL} was not available in one patient due to technical failure (C). K^{trans} could not be assessed in one patient due failed fat saturation (K). PARP: poly (ADP-ribose) polymerase.

Europe PMC Funders Author Manuscripts

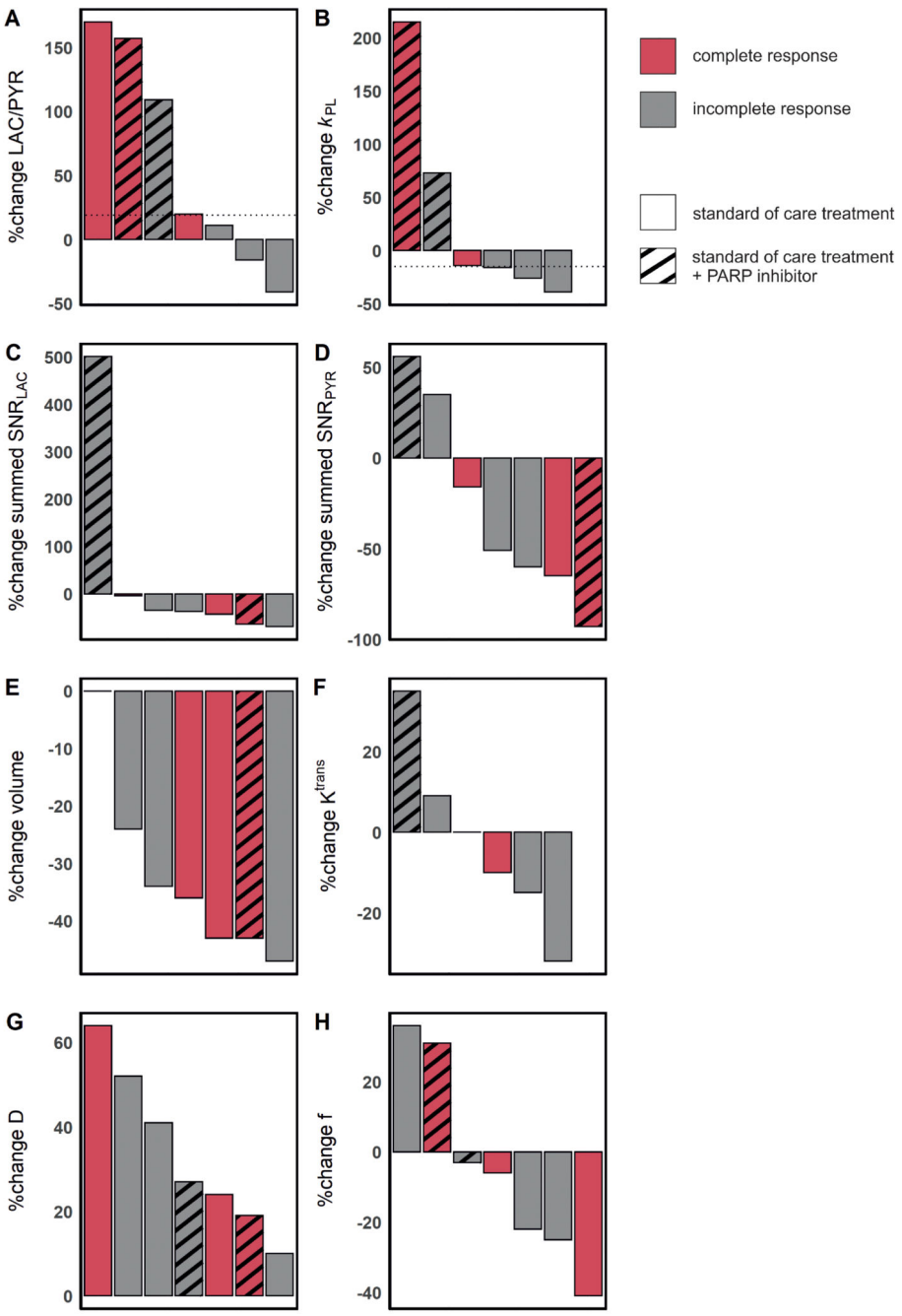

Figure 4. Changes in hyperpolarized ^{13}C-MRI and ^{1}H-MRI parameters in seven patients with complete and incomplete responses.

Results are shown for standard-of-care treatment with and without PARP inhibitor treatment. (A) A threshold of +20% change in LAC/PYR distinguished responders from non-responders on standard-of-care therapy (shown with a dashed horizontal line). One non-responder receiving PARP inhibitor treatment also showed an increase in LAC/PYR of ≥20%, which may be explained by NAD^+ availability (see main text). (B) A threshold set at a -15% change in k_{PL} (dashed horizontal line) distinguished responders from non-responders on standard-of-care therapy. A patient receiving PARP inhibitor treatment in

addition but demonstrating pCR also showed a change in k_{PL} above this threshold. k_{PL} was not available for one patient due to a technical failure. (C-H) There were no thresholds that could be used to distinguish pCR from non-pCR for any of the remaining ^{1}H-MRI or ^{13}C-MRI parameters. Change in K^{trans} was not evaluable for one patient where fat saturation failed at baseline.

Europe PMC Funders Author Manuscripts

Europe PMC Funders Author Manuscripts

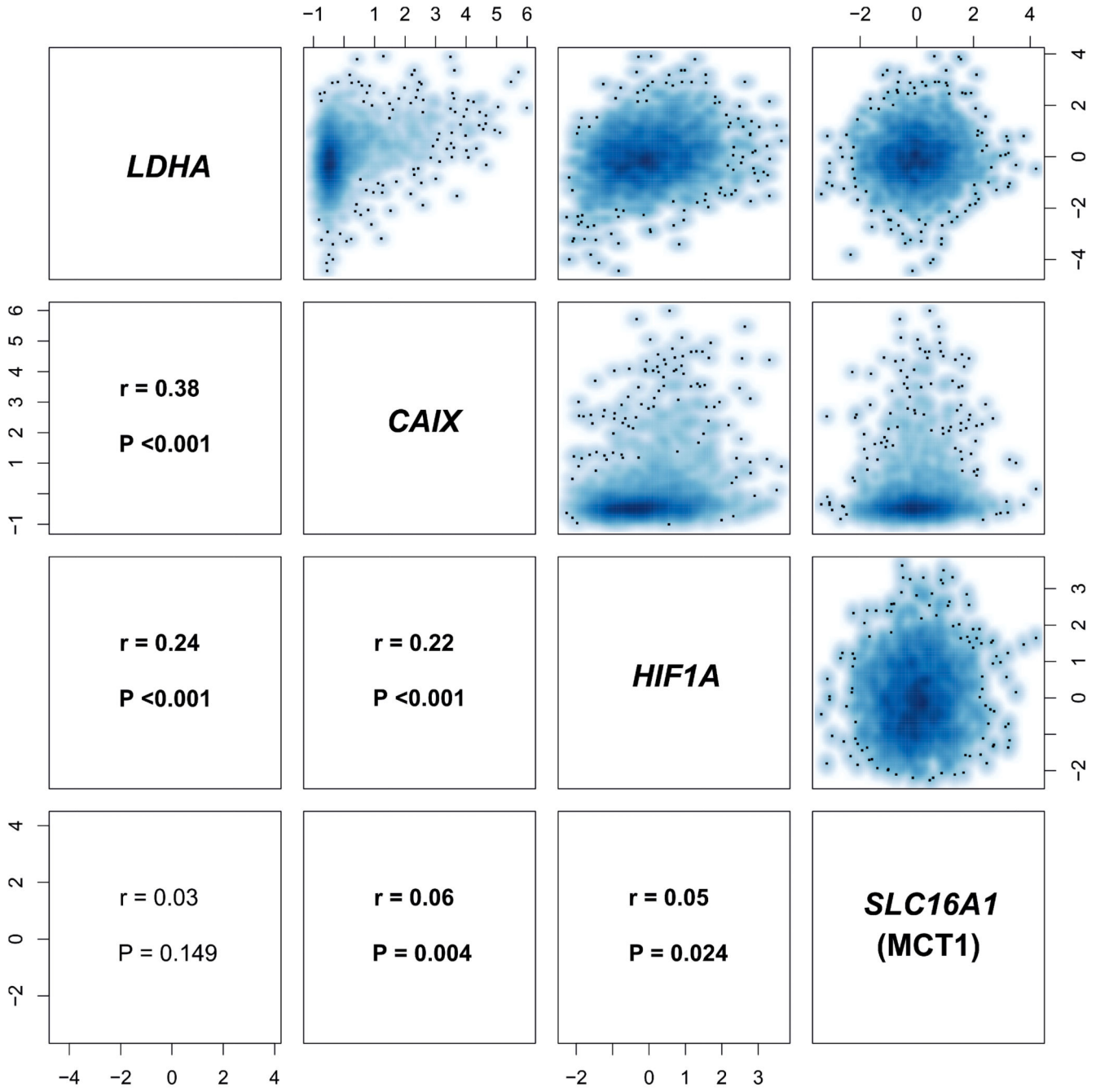

Figure 5. Correlation matrix of *LDHA*, *SLC16A1* (MCT1), *CAIX*, and *HIF1A* expression in METABRIC.

There is a significant correlation between *LDHA* and *SLC16A1* (MCT1) expression (z-scores) with the hypoxia markers *CAIX* and *HIF1A*. r: Pearson correlation coefficient.

Europe PMC Funders Author Manuscripts

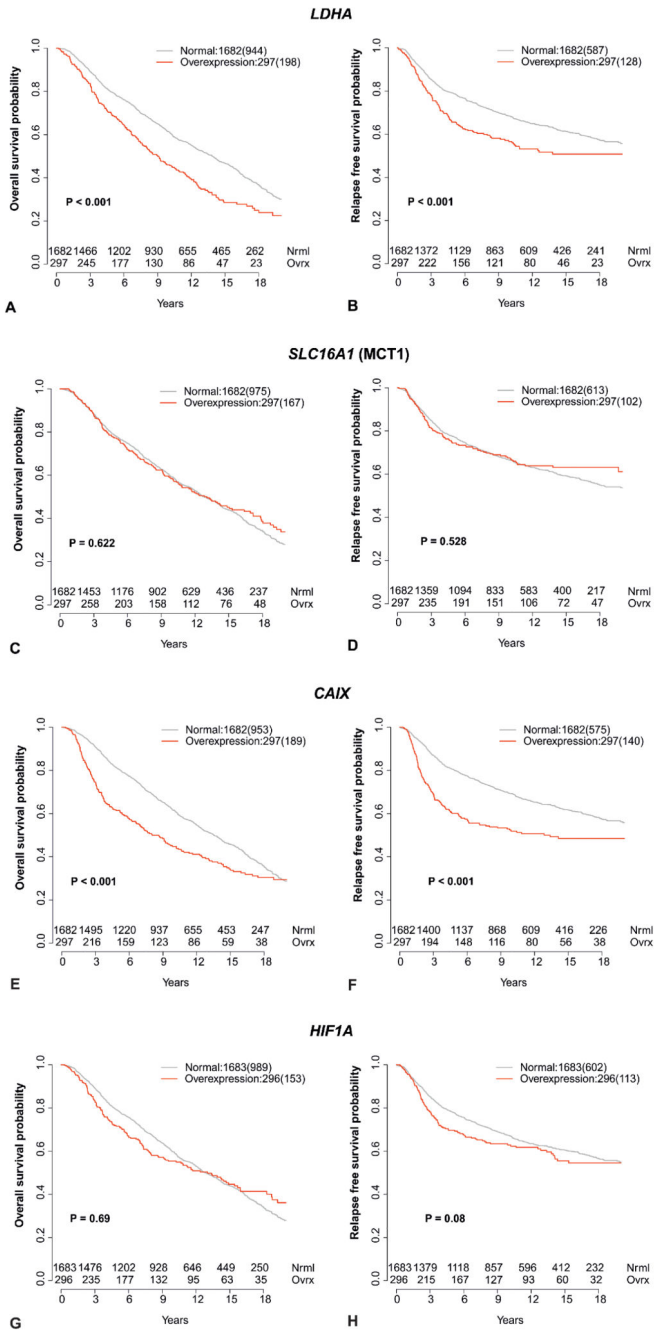

Figure 6. Correlation of *LDHA*, *SLC16A1* (MCT1), *CAIX*, and *HIF1A* expression with survival in METABRIC.

Kaplan-Meier curves for normal expression and overexpression (85th percentile) of *LDHA* (A and B), *SLC16A1* (MCT1) (C and D), *HIF1A* (E and F), and *CAIX* (G and H). The left column shows overall survival and the right column relapse free survival. Number of events are shown in brackets.